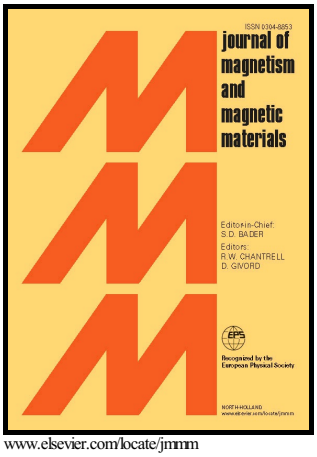

www.elsevier.com/locate/jmmm

Flux growth and characterization of Ce- substituted $_{Nd2Fe14}$B single crystals

Michael A. Susner, Benjamin S. Conner, Bayrammurad I. Saparov, Michael A. McGuire, Ethan J. Crumlin, Gabriel M. Veith, Huibo Cao, Kavungal V. Shanavas, David S. Parker, Bryan C. Chakoumakos, Brian C. Sales

PII: S0304-8853(16)32772-X
DOI: http://dx.doi.org/10.1016/j.jmmm.2016.10.127
Reference: MAGMA62040

To appear in: *Journal of Magnetism and Magnetic Materials*

Received date: 9 March 2016
Revised date: 26 August 2016
Accepted date: 25 October 2016

Cite this article as: Michael A. Susner, Benjamin S. Conner, Bayrammurad I Saparov, Michael A. McGuire, Ethan J. Crumlin, Gabriel M. Veith, Huibo Cao, Kavungal V. Shanavas, David S. Parker, Bryan C. Chakoumakos and Brian C Sales, Flux growth and characterization of Ce- substituted $_{Nd2Fe14}$B singl crystals, *Journal of Magnetism and Magnetic Materials* http://dx.doi.org/10.1016/j.jmmm.2016.10.127

Flux Growth and Characterization of Ce- Substituted $Nd_2Fe_{14}B$ Single Crystals

Michael A. Susner[a], Benjamin S. Conner[a], Bayrammurad I. Saparov[a,d], Michael. A. McGuire[a], Ethan. J. Crumlin[b], Gabriel M. Veith[a], Huibo. Cao[c], Kavungal V. Shanavas[a], David S. Parker[a], Bryan C. Chakoumakos[c], Brian C. Sales[a]

[a]*Materials Science and Technology Division, Oak Ridge National Laboratory, Oak Ridge, Tennessee 37831 USA*
[b]*Advanced Light Source, Lawrence Berkeley National Laboratory, Berkeley, California 94720 USA*
[c]*Quantum Condensed Matter Division, Oak Ridge National Laboratory, Oak Ridge, Tennessee 37831 USA*
[d]*Now with the Department of Mechanical Engineering and Materials Science and the Department of Chemistry, Duke University, Durham, North Carolina 27708 USA*

Abstract

Single crystals of $(Nd_{1-x}Ce_x)_2Fe_{14}B$, some reaching $\sim 6 \times 8 \times 8$ mm^3 in volume, are grown out of Fe-(Nd,Ce) flux. This crystal growth method allows for large $(Nd_{1-x}Ce_x)_2Fe_{14}B$ single crystals to be synthesized using a simple flux growth procedure. Chemical and structural analyses of the crystals indicate that $(Nd_{1-x}Ce_x)_2Fe_{14}B$ forms a solid solution until at least $x = 0.38$ with a Vegard-like variation of the lattice constants with x. Refinements of single crystal neutron diffraction data indicate that Ce has a slight site preference (7:3) for the $4g$ rare earth site over the $4f$ site. Magnetization measurements at 300 K show only small decreases with increasing Ce content in saturation magnetization (M_s) and anisotropy field (H_A), and Curie temperature (T_C). First principles calculations are carried out to understand the effect of Ce substitution on the electronic and magnetic properties. For a multitude of applications, it is expected that the advantage of incorporating lower-cost and more abundant Ce will outweigh the small adverse effects on magnetic properties. Ce-substituted $Nd_2Fe_{14}B$ is therefore a potential high-performance permanent magnet material with substantially reduced Nd content.

Keywords:
Permanent Magnets, $Nd_2Fe_{14}B$, Rare Earth Magnets, Single Crystal Synthesis, Neutron Diffraction

PACS: 75.50.Cc, 75.50.Vv, 75.50.Ww, 71.20.Eh

1. Introduction

The reduction of critical materials present in consumer and industrial products in general, and in rare earth (RE) -based permanent magnets in particular, is a pressing concern due to increasing demand and a decline and/or uncertainty in the supply chain of these materials. Dysprosium, judged to be the most critical of these elements [1], is substituted onto the Nd site in $Nd_2Fe_{14}B$ (2-14-1) permanent magnets to increase the value of their coercive field and maximum operating temperatures [2, 3]. Depending on the application, the amount of Dy added can be large, in the range of 1.4-8.7 wt% [1]. The highest temperature applications, those that rely on the greatest quantities of dysprosium, are required by the rapidly emerging technologies of wind turbines, magnetically levitated transport, and traction motors for hybrid and electric cars [1].

Though Dy is indeed considered the most critical element, by many criteria Nd is not that far behind on the list of these crucial energy materials [1]. It is therefore imperative that new and innovative solutions are applied to the synthesis of permanent magnets that contain more abundant elements. To this end, recent work by Pathak *et al*. [4] has shown that partial substitution of Ce for Nd and Co for Fe (*i.e*. $(Nd_{0.8}Ce_{0.2})_2Fe_{12}Co_2B$) results in a permanent magnet with properties superior to those of Dy-substituted 2-14-1 magnets for temperatures above 450 K. However, these samples were fabricated as die-upset, hot-pressed, or melt-spun ribbons where the exhibited properties are dependent on such extrinsic factors as microstructure and secondary phases. Since 1) Ce is by far the most abundant of the rare earth elements and 2) these new magnets simultaneously eliminate the need for Dy and reduce the amount of Nd used, they

Email address: author to whom correspondence should be addressed at susnerma@ornl.gov (Michael A. Susner)

represent an exciting opportunity for the development of lower-cost high performance permanent magnets. The growth of single crystals helps us understand the intrinsic properties of these materials.

The crystal structure of $Nd_2Fe_{14}B$ was established as tetragonal (space group $P4_2/mnm$, No. 136) as early as 1984 by Givord *et al.*[5], Herbst *et al.* [6], and Shoemaker *et al.* [7]. There are two separate and inequivalent RE sites; represented by their respective Wyckoff symbols, one is a $4g$ site and the other a $4f$ site. Also present are six inequivalent Fe sites and one B site. Past investigations as to the effects of chemical substitution of different RE elements onto the Nd site are numerous; see the review article by Herbst [8] and the references therein. However, detailed, quantitative experimental studies on the effects of Ce substitution of varying amounts in pure single crystal samples have not previously been performed. Abache and Osterreicher [9] studied aligned powders to determine the crystal structure, magnetic anisotropy, and spin reorientation temperature in $(Nd_{1-x}Ce_x)_2Fe_{14}B$ for $x = 0.25$ and $x = 1$ along with a multitude of other compositional variations of $Nd_2Fe_{14}B$ achieved by changing the degree and type of substitutions on the RE and transition metal (TM) sites. However, no detailed study was made concerning the magnetic properties as a function of Ce concentration in that work. They also do not make any claims whatsoever as to the stability of the $(Nd_{1-x}Ce_x)_2Fe_{14}B$ compound for $0.25 \leq x \leq 1$. More recently, density functional theory calculations of Alam *et al.* [10] actually predict a phase segregation for $x \geq 0.3$ in $(Nd_{1-x}Ce_x)_2Fe_{14}B$. Pathak *et al.* [4] have experimentally observed phase segregation under the conditions required for the fabrication of melt-spun ribbons.

Information also of interest in the $(Nd_{1-x}Ce_x)_2Fe_{14}B$ system is the site preference of the Ce as there are two structurally distinct RE sites. Previous theoretical predictions about Ce site preference exist [9, 10], but direct experimental evidence to determine whether Ce in $(Nd_{1-x}Ce_x)_2Fe_{14}B$ is preferentially associated with the larger $4g$ site or the smaller $4f$ site has previously been lacking.

The $(Nd_{1-x}Ce_x)_2Fe_{14}B$ system has recently come under much attention. Experimental investigations by Gschneidner *et al.* discovered an anomaly evident in the plot of the c lattice parameter vs. Ce concentration in polycrystalline $(Nd_{1-x}Ce_x)_2Fe_{14}B$ alloys for $x \approx 0.2$ [11]. Similar anomalies were evident in plots of coercivity (H_c), maximum energy product (BH_{max}), and remnant magnetization (B_r) as functions of Ce concentration, along with the aforementioned phase segregation. The same investigation yielded an extraordinary result: when Co is substituted for Fe by two atoms per formula unit in the $(Nd_{1-x}Ce_x)_2Fe_{14-y}Co_yB$ polycrystalline materials, where $x = 0.20$, the Curie temperature (T_C) increased by 150 K while room temperature coercivity dropped only 22% as compared to an equivalent sample with no Co doping, *i.e.* $x = 0.2, y = 0$. The anisotropy field (H_A), saturation moment (M_s), and B_r remained more or less unchanged compared to the $x = 0.2, y = 2$ case. The possible application of such excellent Dy-free magnets opens an exciting line of research focused on linking the microscopic magnetic properties in pure crystalline samples with the macroscopic magnetic properties of bulk permanent magnets.

In the current work, we have employed single crystal growth techniques to synthesize single crystals of Ce-doped 2-14-1 compounds. We show here observations contrary to those of the melt-spun ribbons of Pathak *et al.* [4] for our samples grown under the slow crystallizing conditions of flux growth; we are able to stabilize uniform single crystals of $(Nd_{1-x}Ce_x)_2Fe_{14}B$ for values $0 \leq x \leq 0.38$. Furthermore, we have used these single crystal specimens together with neutron diffraction to experimentally determine that Ce has a slight site preference in the 2-14-1 structure for the larger RE $4g$ site [9, 10]. Next, we have also measured important magnetic properties such as M_s, T_C, H_A etc. for $(Nd_{1-x}Ce_x)_2Fe_{14}B$ for the composition range $0 \leq x \leq 0.38$. Finally, we conclude this report with first principles density functional theory calculations which help explain the causes of the changes in M_s, T_C, and H_A with Ce substitution. These investigations are an important first step in elucidating the physics behind the economically beneficial, high-performance magnetic properties observed by Pathak *et al.*[4]

2. Experimental Details

Single crystals of both $Nd_2Fe_{14}B$ and $NdFe_4B_4$ type materials were grown from Nd-Fe flux following the techniques originally reported by Canfield *et al.* [12, 13]. The starting materials were cuttings of high purity metals: Ce (Ames Laboratory, 99.99%), Nd (Ames Laboratory, 99.99%), Fe (Alfa Aesar, 99.98%), and isotopically pure ^{11}B (^{11}B, ORNL, 99.99+%). The use of ^{11}B was necessary for neutron diffraction experiments as ^{10}B is exceptionally good at neutron capture. Appropriate stoichiometries of these elements (see Table 1) were loaded into Ta crucibles (1.25 cm diameter, 7 cm length) and sealed under ~0.5 atm Ar using an arc-melter. A Ta frit was placed above the starting materials to act as a filter during the centrifugation process.

Table 1: Molar Ratios for Sample Fluxes and Compositions of Single Crystals as Determined from EDS.

Flux Composition (molar percent)				Composition of	Composition of
Nd	Ce	Fe	^{11}B	2-14-1 phase	1-4-4 phase
51	0	43.3	5.8	$Nd_2Fe_{14}{}^{11}B$	$NdFe_4{}^{11}B_4$
43.3	7.7	43.3	5.8	$(Nd_{0.911(14)}Ce_{0.089(7)})_2Fe_{14}{}^{11}B$	$Nd_{0.904(9)}Ce_{0.096(1)}Fe_4{}^{11}B_4$
32.9	18.1	43.3	5.8	$(Nd_{0.78(4)}Ce_{0.22(1)})_2Fe_{14}{}^{11}B$	$Nd_{0.75(9)}Ce_{0.25(3)}Fe_4{}^{11}B_4$
25.5	25.5	43.3	5.8	$(Nd_{0.62(6)}Ce_{0.38(4)})_2Fe_{14}{}^{11}B$	$Nd_{0.61(3)}Ce_{0.39(2)}Fe_4{}^{11}B_4$
18.1	32.9	43.3	5.8	–	$Nd_{0.49(2)}Ce_{0.51(2)}Fe_4{}^{11}B_4$

The Ta crucibles were subsequently sealed in quartz ampoules under ~1/3 atm Ar.

The sealed ampoules were placed into a large box furnace and heated to 1190 °C over 12 h and held at that temperature for 24 h. The furnace was then cooled to 800 °C over 390 h, after which the samples were removed and the flux was decanted using a centrifuge. Large, single crystal specimens (some ~1 g) of the $Nd_2Fe_{14}B$ (2-14-1) phase (Fig. 1a, inset) and smaller elongated prisms (~ 2 mm × 2 mm × 10 mm) of the $NdFe_4B_4$ (1-4-4) phase were extracted from the crucibles. The ultimate sizes of the 2-14-1 crystals were not influenced by the compositions of the fluxes with the exception of the largest Ce concentration (in this case, large crystals of the Laves phase compound $Ce_{0.85}Nd_{0.15}Fe_2$ formed rather than the 2-14-1 phase). The crystallographic faces of all phases present after decanting were well-defined. In Fig. 1a we present XRD reflections resulting from a (0 0 l) face of the undoped $Nd_2Fe_{14}B$ sample.

Analyses of elemental compositions were performed using a Hitachi TM-3000 electron microscope equipped with a Bruker Quantax 70 energy dispersive (EDS) X-ray spectrometer (*c f*. Table 1). To determine the average composition and its error for each sample we have taken EDS data using 6-12 separate spots over 2-3 different crystals. For all compositions small crystals were ground into powder and used to produce XRD patterns using a PANalytical XPert Pro diffractometer (Cu K_α, 1.5406 Å). The resultant reflections were analyzed for lattice parameters using the LeBail fitting function available with the onboard HighScore Plus software package. Single crystal diffraction was performed using a Rigaku single crystal X-ray diffractometer with Dectris Pilatus 200K detector (Mo K_α, 0.71073 Å); the resultant diffraction patterns were analyzed using the onboard Rigaku software with absorption corrections performed using a spherical approximation. The structure was refined using SHELX (Ref. [14]) with WinGX. Single crystal neutron diffraction was measured using the HB-3A four circle diffractometer at the High Flux Isotope Reactor (HFIR) at the Oak Ridge National Laboratory. The ~300 mg sample was measured at 4 K and 300 K by neutrons with a wavelength of 1.003 Å from a bent Si-331 monochromator [15]. The structure was refined using the FULLPROF software package [16].

X-ray photoelectron spectroscopy (XPS) data were collected with a PHI 3056 XPS spectrometer with an Al K_α source (1.4866 keV) in a cryo-pumped ultra-high vacuum chamber with a pressure of $<< 10^{-8}$ Torr. Fresh surfaces of the crystal were created by grinding a single crystal in an Ar-filled glove box and transferring to the XPS chamber using a vacuum transfer system. Synchrotron data was taken at the Advanced Light Source (ALS) at the Lawrence Berkeley National Laboratory (Berkeley, USA) using Beamline 9.3.1. This beam-line is a bent magnet beam-line with an energy range of 2.3−5.2 keV. The minimal spot size at the beam-line is 0.7 mm (v) × 1.0 mm (h) [17].

Magnetic properties were measured using 1) a Quantum Design Magnetic Property Measurement System (MPMS) and 2) the DC-extraction capability of the AC Measurement System (ACMS) option of a 14 T Quantum Design Physical Property Measurement System (PPMS). To measure the magnetization along the easy direction as a function of magnetic field 1) a *c* axis face was found on a single crystal using the X-ray diffractometer, 2) the crystal was polished into a parallelepiped with a long axis aligned with either the *a* or *c* direction (for hard and easy axis measurements, respectively) and 3) the crystal segments were placed into the MPMS or PPMS under magnetic fields of up to 13 T. The hard axis measurements were found by grinding small crystals of each composition into powder and placed into a gel cap with epoxy; the epoxy was allowed to set under an applied magnetic field so as to align the

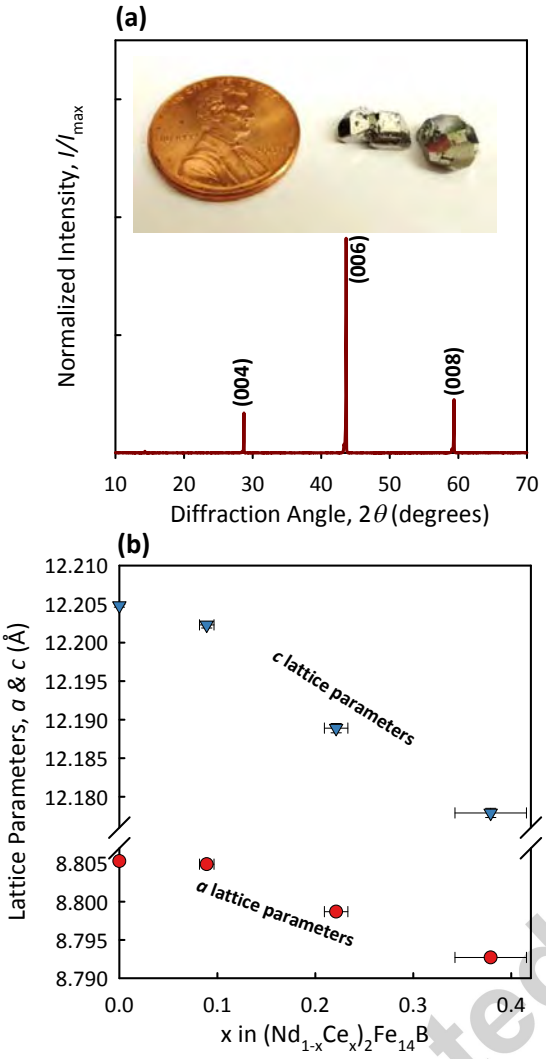

Figure 1: (a) XRD diffraction pattern from (0 0 l) face of undoped $Nd_2Fe_{14}B$ crystal. The inset shows a size comparison image of crystals of the same composition. (b) Lattice parameters of the 2-14-1 phase plotted against Ce concentration. The error bars for the abscissa represent the errors given in the EDS analysis in Table 1.

powders. Measurements were taken with H oriented perpendicular to the easy direction at 5 K, 300 K, and 400 K. To obtain a correct value for the saturation magnetization a measurement of the same gel cap was taken with H oriented parallel to the easy direction; these data were then normalized to the values obtained from the single crystal easy axis measurements. The easy axis measurements of the aligned powder samples and the single crystal specimens were in good agreement. All magnetization data were corrected by applying a demagnetization factor based on the respective sample geometries.

The $M(T)$ properties of the 2-14-1 crystals were also measured using the Quantum Design MPMS. The magnetization was measured as a function of temperature using an applied magnetic field of 10^3 Oe; temperature ranges were 2 K $\leq T \leq$ 750 K. Further confirmation of the Curie temperatures of the grown ferromagnetic crystals was obtained through thermal analysis using a Perkin Elmer Pyris Diamond Thermo-Gravimetric Analyzer/ Differential Thermal Analyzer (TGA/DTA).

The first principles calculations are carried out within density functional theory (DFT). We use the generalized gradient approximation [18] within the projector augmented wave method [19] as implemented in the Vienna *ab initio* simulation package [20, 21]. An energy cutoff of 400 eV and k space sampling on a $7 \times 7 \times 5$ grid are employed. The Ce substitution on the Nd site is handled by the virtual crystal approximation (VCA).

3. Results

3.1. Crystal growth and Ce doping

The as-grown crystals displayed well-defined faceting (Fig. 1a, inset). The sizes of the 2-14-1 crystals were typically $\sim 2 \times 2 \times 2$ mm^3 with some reaching $\sim 6 \times 8 \times 8$ mm^3 in volume. Except for the growth with a nominal flux composition of 18.1% Nd and 32.9% Ce where a Laves phase compound formed rather than the 2-14-1 phase, all resulting single crystals were of similar size. The 1-4-4 phases grew as needles $\sim 1 \times 1 \times 10$ mm^3 and will be the subject of a forthcoming publication.

Through EDS analysis, we were able to measure the relative concentrations of the rare earths (RE) and transition metals (TM). The boron content could not be reliably estimated from the EDS measurements. A variety of growths were used to maximize the Ce concentrations within the crystals. Results suggest that $x = 0.38$ is the maximum attainable by this synthesis route.

3.2. Structural characterization

The room temperature powder XRD patterns were taken of the 2-14-1 phases using the powder from ground crystals. LeBail fitting was used to extract the lattice parameters, which are plotted in Fig. 1b as functions of Ce concentration. The values of both the a and c lattice parameters decrease monotonically with increasing quantities of Ce (*cf.* Fig. 1b). At $x = 0.38$ in $(Nd_{1-x}Ce_x)_2Fe_{14}B$ we see that the value of a is 0.14% smaller than that of the undoped sample. Similarly, for

Table 2: Summary of 250 K single crystal X-ray diffraction data of sample $(Nd_{0.78}Ce_{0.22})_2Fe_{14}B$;
Space group $P4_2/mnm$; $a = b$=8.8032(13) Å; c=12.1880(20) Å; $\alpha = \beta = \gamma = 90^\circ$

Site	Atomic Coordinates x	y	z	U_{iso} (Å^2)
B1 (4*g*)	0.1239(8)	0.1239(8)	0	0.0121(16)
Fe1 (16k_1)	0.03732(7)	0.35986(7)	0.32411(5)	0.0099(2)
Fe2 (16k_2)	0.06698(7)	0.27578(7)	0.12753(5)	0.099(2)
Fe3 (8j_1)	0.09802(7)	0.09802(7)	0.29599(7)	0.0105(2)
Fe4 (8j_2)	0.31758(7)	0.31758(7)	0.25407(7)	0.0103(2)
Fe5 (4*e*)	0	0	0.11514(10)	0.0098(3)
Fe6 (4*c*)	0	0.5	0	0.0105(3)
Nd1/Ce1 (4*g*)	0.22992(4)	0.77008(4)	0	0.0108(2)
Nd2/Ce2 (4*f*)	0.35743(4)	0.35743(4)	0	0.0108(2)

Reliability factors	*R*1	*wR*2	R_{int}	GOF
	0.0505	0.1189	0.0936	0.882

Table 3: Summary of 110 K single crystal X-ray diffraction data of sample $(Nd_{0.78}Ce_{0.22})_2Fe_{14}B$;
Space group $P4_2/mnm$; $a = b$=8.8041(13) Å; c=12.1633(17) Å; $\alpha = \beta = \gamma = 90^\circ$

Site	Atomic Coordinates x	y	z	U_{iso} (Å^2)
B1 (4$_g$)	0.1221(14)	0.1221(14)	0	0.008(3)
Fe1 (16k_1)	0.03717(14)	0.36003(14)	0.32427(10)	0.0093(4)
Fe2 (16k_2)	0.06714(14)	0.27523(14)	0.12785(11)	0.0102(4)
Fe3 (8j_1)	0.09839(14)	0.09839(14)	0.29627(16)	0.0108(4)
Fe4 (8j_2)	0.31744(13)	0.31744(13)	0.25413(14)	0.0102(4)
Fe5 (4$_e$)	0	0	0.1155(2)	0.0104(5)
Fe6 (4$_c$)	0	0.5	0	0.0101(6)
Nd1/Ce1 (4*g*)	0.23015(7)	0.76985(7)	0	0.0102(3)
Nd2/Ce2 (4*f*)	0.35750(7)	0.35750(7)	0	0.0102(3)

Reliability factors	*R*1	*wR*2	R_{int}	GOF
	0.0792	0.1849	0.0964	1.196

the same composition, c is 0.22% smaller. No anomalies are present in the lattice parameters as a function of Ce content, in contrast to polycrystalline samples of the same composition synthesized by Pathak *et al*. [4] where a two-phase region was observed for $0.15 < x < 0.4$ in $(Nd_{1-x}Ce_x)_2Fe_{14}B$. However, it should be noted that there is a wide spacing between our data points which could potentially belie small anomalies in the lattice parameters as a function of Ce content. Our single crystal specimens containing the two highest compositions of Ce ($x = 0.22$ and $x = 0.38$) fall within the two phase region suggested by the aforementioned authors, indicating that the range of solid solution in this system is sensitive to processing conditions such as temperature and solidification rate. Single crystal X-ray diffraction on the sample with composition $(Nd_{0.78}Ce_{0.22})_2Fe_{14}B$ was performed at 250 K and 110 K; these temperatures bracket the spin reorientation temperature of ~140 K in $Nd_2Fe_{14}B$ [9, 22]. Structural refinements were made using SHELX [14] from 1068 and 966 unique reflections, respectively, and are presented in Tables 2 and 3. The space group matched that of previous reports and the powder diffraction data, $P4_2/mnm$. The values of the lattice parameters from the single crystal data match well with those obtained from powder diffraction. No discernible structural difference was seen between the data collected above the spin reorientation temperature and that collected below it. For the single crystal X-ray diffraction analyses no attempts were made to refine the Nd/Ce occupancy as the scattering factors of the two RE elements were too similar. However, the neutron scattering lengths for Nd (7.69 fm) and Ce (4.84 fm) allow for excellent fidelity to refine the site occupancies. Later refinements using the occupancy results elucidated from this neutron diffraction data (Table 4) yielded no change in the single crystal XRD refinements. The structure derived from the 250 K single crystal XRD refinement matches well with that published in the literature [6, 8, 23, 24, 25].

Single crystal neutron diffraction was performed on a ~300 mg sample of $(Nd_{0.78}Ce_{0.22})_2Fe_{14}B$ at a temperature of 300 K; 630 reflections were collected. The magnetic signals were found with a propagation vector of $\vec{k} = 0$, i.e., they coincide with the nuclear peaks, as expected for a ferromagnet. Therefore, in the data refinements, the nuclear and magnetic structure parameters were refined together. The thermal parameters were determined from our single-crystal X-ray data and fixed in the neutron refinements. Site occupancies were determined by first assuming uniform distribution of Ce and Nd on the 4f and 4g sites and then allowing Ce/Nd to migrate from one site to the next. Refinements were attempted for two cases: 1) where Ce carries a moment and 2) where Ce does not carry a moment. The resulting site occupancies did not change between these two refinements. The neutron diffraction refinement results are presented in Table 4.

Given the fact that the easy axis of this material is along the [0 0 1] direction [8], the magnetic vectors at 300 K were constrained to lie along this vector to reduce the total number of refined parameters. At 300 K the total refined magnetic moment is 38 ± 3 μ_B/f.u., in reasonable accord with the MPMS-determined value of 32.3 μ_B/f.u. Magnetic refinements on ferromagnets using unpolarized neutron diffraction data make refinements on each magnetic site have an accuracy no better than μ_B/f.u. In addition, imperfectly corrected system-

Table 4: Summary of 300 K single crystal neutron diffraction data of sample $(Nd_{0.78}Ce_{0.22})_2Fe_{14}B$. The magnetic moments are aligned along the *c*-axis. The atomic environment describes all neighbors within 4 Å.

		Atomic Coordinates						
Lattice Constants	**Site**	*x*	*y*	*z*	U_{iso} (Å^2)	**Occ. f.**	**Moment (μ_B)**	**Atomic Environment**
$a = b = 8.8032(10)$Å	B1 (4*g*)	0.12427(33)	0.12427(33)	0	0.0110(8)	1	–	12 Fe, 3 Nd, 1 B
$c = 12.1880(10)$Å	Fe1 (16k_1)	0.03748(14)	0.35958(13)	0.32422(9)	0.0081(3)	1	2.9(1)	11 Fe, 2 Nd, 1 B
$\alpha = \beta = \gamma = 90°$	Fe2 (16k_2)	0.06709(14)	0.27576(14)	0.12751(9)	0.0081(3)	1	2.3(1)	10 Fe, 2 Nd
	Fe3 (8j_1)	0.09784(14)	0.09784(14)	0.29588(13)	0.0081(3)	1	1.6(2)	9 Fe, 3 Nd, 1 B
$P4_2/mnm$	Fe4 (8j_2)	0.31749(14)	0.31749(14)	0.25434(13)	0.0081(3)	1	2.3(2)	12 Fe, 2 Nd, 1 B
	Fe5 (4*e*)	0	0	0.11502(20)	0.0081(3)	1	3.2(2)	13 Fe, 2 Nd, 2 B
Total Moment	Fe6 (4*c*)	0	0.5	0	0.0081(3)	1	1.3(1)	8 Fe, 4 Nd, 2 B
$38 \pm 3\ \mu_B$	Nd1 (4*g*)	0.23026(27)	0.76974(27)	0	0.0079(5)	0.69(2)	3.4(1)	16 Fe, 2 Nd, 2 B
	Ce1 (4*g*)	0.23026(27)	0.76974(27)	0	0.0079(5)	0.31(2)	–	16 Fe, 2 Nd, 2 B
	Nd2 (4*f*)	0.35690(27)	0.35690(27)	0	0.0079(5)	0.87(2)	1.8(1)	16 Fe, 3 Nd, 1 B
	Ce2 (4*f*)	0.35690(27)	0.35690(27)	0	0.0079(5)	0.13(2)	–	16 Fe, 3 Nd, 1 B

Reliability factors	R_{F^2}	wF^2	R_F	χ^2
	0.0473	0.0775	0.0461	4.06

atic errors could also add error to the refinement [26]. The Fe sites have moments ranging from 1.3(1)−3.2(2) μ_B. This variability is likely caused by the different steric environments experienced by each of the different Fe sites. In Table 4 we list the atomic neighbors out to a distance of 4 Å together with the neutron diffraction data for comparison. As is evident from the data, the refined moments on the Fe sites scale well with the amount of Fe coordination [27]. For example, the three largest Fe moments are seen on the 4*e*, 16k_1, and 8j_2 sites which have Fe coordinations of 13, 11, and 12, respectively. The smallest moment is observed at the Fe 4*c* site (Fe coordination of 8) which also experiences the highest degree of RE coordination, with 4 of the 12 nearest neighbors being Nd/Ce. Of course the magnitude of the moment is not dependent on Fe coordination alone. Isnard and Fruchart [28] have shown that Fe-B bonds lead to lower moments (e.g. the 4*e* and 16k_1 positions), though in $Nd_2Fe_{14}B$ this effect is compensated by the presence of a large number of ligand lines or sharing of nearest-neighbor atoms with central atoms in the structure which can serve to increase the moment on a given site [29, 30]. The two RE sites have moments of 2.4 and 1.6 μ_B for the 4*g* and 4*f*, respectively. Although one should expect the lower moment to lie on the site with the greater Ce occupancy, the available room temperature neutron diffraction data in the literature showing separate refinements of the moments for the different RE sites in undoped $Nd_2Fe_{14}B$ also show an intrinsically lower moment on the 4*f* site [27, 31]. Herbst *et al*. [27] have suggested that the fact that the 4*f* site has two of the low-moment Fe 4*e* sites as neighbors could contribute to the difference in moment between the two RE sites (observed to be greater at 77 K), but no mechanism was advanced.

With respect to RE occupancy, the 4*g* site is, in terms of size, the larger of the two sites and is therefore predicted to be preferred for Ce, assuming the Ce is in the +3 oxidation state [10]. For 12-fold coordination, the Ce^{3+} ion (1.825 Å diameter) is larger than the Ce^{4+} ion (1.715 Å) [32] and is therefore likely to prefer this larger site. In comparison, for the same coordination, Nd has an effective radius of 1.821 Å. When requiring that the thermal displacement parameters for the two different rare earth sites be equal, our 300 K refinements presented in Table 4 show that this preference is not absolute in that Ce site preference for the 4*g* site is 70%. Though the degree of Ce preference for the 4*g* site and the atomic displacement parameters are highly correlated in these refinements, the fact that Ce prefers the 4*g* site does not change. These observations concur with the preliminary XPS data taken at the Advanced Light Source (ALS) at the Lawrence Berkeley National Laboratory whereby the XPS spectrum for the Ce 3*d* electrons most closely resembles that of Ce_2O_3, indicating that the majority of Ce is in the +3 oxidation state for this composition. Further experimentation is necessary to confirm this initial result.

3.3. Spin reorientation temperature

Using single crystal neutron diffraction, the (006) reflection of $(Nd_{1-x}Ce_x)_2Fe_{14}B$ was measured upon warming (Fig. 2). Referring to Fig. 2, we see at 130.5 K a noticeable increase in the (006) peak intensity is evident, representing the spin reorientation transi-

tion whereby the magnetization easy axis shifts from the [0 0 1] direction at high temperatures to something near the [3 3 5] direction at low temperatures. Previous investigations of undoped $Nd_2Fe_{14}B$ by Abache and Oesterreicher [9, 22] attributed this reorientation to competing anisotropies of the 4*g* and 4*f* RE sites. In their argument, the 4*f* site (the smaller of the two) is more susceptible to planar moment alignment. At temperatures above the spin reorientation temperature (T_s) the axial anisotropies of the RE and TM sites force the 4*f* site to align axially in a ferromagnetic structure. However, below 140 K the preference of the 4*f* site to align its moment in a planar orientation is much stronger compared to the competing influences of the Fe sites, resulting in spin reorientation and a new easy axis for the system about 49° canted away from the *c* axis [9, 22, 33]. The spin reorientation is therefore dependent on the 4*f* site. The related compound $Ce_2Fe_{14}B$ exhibits no spin reorientation [9] implying that Ce has no inclination for planar orientation of its moment. Substituting Ce on the 4*f* site is expected to affect the spin-reorientation. Previous analysis on pure-phase $Nd_2Fe_{14}B$ single crystals by Wolfers *et al*. [33] details this transition and the accompanying lowering of crystal symmetry associated with it.

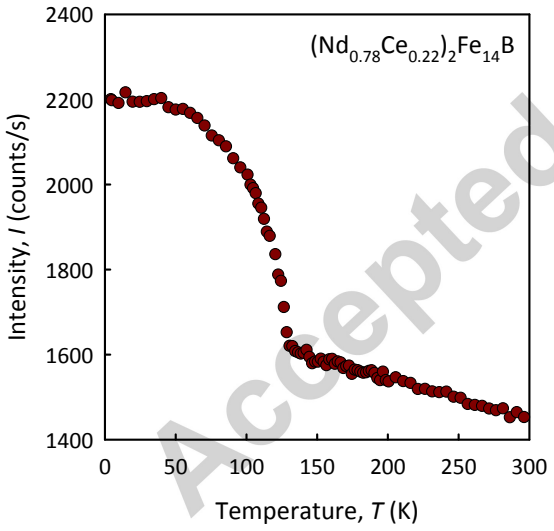

Figure 2: Changes in (006) reflection intensity as measured from 4-300 K using single crystal neutron diffraction on sample with composition $(Nd_{0.78}Ce_{0.22})_2Fe_{14}{}^{11}B$.

In Fig. 3a we plot the magnetization of undoped $Nd_2Fe_{14}B$ as a function of temperature and see increases in magnetization at 586 K and 144 K associated with T_C and T_s, respectively. In Fig. 3b we plot the evolution of T_s as a function of Ce doping. From the neutron diffraction refinements we know that ~13% of the RE 4*f* site is substituted by Ce for the sample with the composition $(Nd_{0.78}Ce_{0.22})_2Fe_{14}B$. Presumably similar levels of Ce are found at this site for the other Ce compositions investigated concomitant with the level of Ce introduced. The spin reorientation temperature is decreased by only about 6% when 38% of the Nd is replaced by Ce. However, the spin reorientation is absent for 100% Ce substitution. This suggests that T_s is suppressed much more rapidly with *x* for larger *x*. This observed weak dependence of T_s on Ce concentration at low *x* and inferred strong dependence of T_s on Ce concentration at high *x* [34] implies that at low *x* we are populating the RE site that does not drive the spin reorientation, consistent with the proposal that the 4*f* site is responsible for the spin-reorientation[9, 22] and our neutron diffraction results that show Ce prefers the 4*g* site. However, the fact that there is some dependence of T_s on *x* (Fig. 3b) implies that the preference of Ce for the 4*g* site is not absolute, consistent with our neutron diffraction data.

3.4. Magnetic properties: Curie temperature, anisotropy field, and saturation magnetization

Relevant magnetic properties are summarized in Table 5. The Curie temperatures of the Ce-substituted 2-14-1 samples were measured via MPMS and DTA/TGA. A permanent magnet affixed to the exterior of the sample chamber was used to produce a magnetic field gradient at the sample such that a change in magnetic susceptibility produced a change in the apparent sample weight. The data from these analyses show a steady monotonic decrease in T_C with increasing Ce concentration. The undoped $Nd_2Fe_{14}B$ yields a T_C of ≈ 584 K, in accord with the established literature value of 585 K [8]. The composition $(Nd_{0.62}Ce_{0.38})_2Fe_{14}{}^{11}B$, on the other hand, shows a T_C of ≈ 544 K, a total decrease of 1.1 K per % Ce substituted. This result is in reasonable accord with a Vegard-like relation existing between the $Nd_2Fe_{14}B$ and $Ce_2Fe_{14}B$ (T_C ≈ 430 K [9, 22]) end members. The values of K_1were estimated from the relation $K_1=\mu_0 H_A M_s/2$, which ignores the small K_2 value of ≈ 0.66 MJ/m^3 reported for $Nd_2Fe_{14}B$ [35]. Our values of K_1(Table 5) largely scale with increasing Ce concentration and tend toward the 300 K value reported for the end-member compound $Ce_2Fe_{14}B$ (1.5 MJ/m^3) at high concentrations [8].

In Fig. 4 we show the *M*(*H*) curves for the four Ce-substituted samples at 300 K, respectively. Both easy-axis and hard-axis measurements are plotted. For $Nd_2Fe_{14}B$ there is no difference in the magnetization reported for the [1 0 0] and [0 1 0] directions [36]; the

Table 5: Magnetic Properties of Ce-substituted $Nd_2Fe_{14}B$

Sample Composition	M_s(400K) [μ_B/f.u.]	M_s(300K) [μ_B/f.u.]	M_s(5 K) [μ_B/f.u.]	T_C(TGA) [K]	T_C(DTA) [K]	T_C(MPMS) [K]	T_s [K]	K_1(300 K) [MJ/m^3]
$Nd_2Fe_{14}{}^{11}B$	29.8	33.6	38.6	583	584	586	143.5	4.9
$(Nd_{0.91}Ce_{0.089})_2Fe_{14}{}^{11}B$	27.9	31.7	35.1	576	575	579	141.4	4.5
$(Nd_{0.78}Ce_{0.22})_2Fe_{14}{}^{11}B$	27.7	32.3	34.9	561	559	561	139.3	4.6
$(Nd_{0.62}Ce_{0.38})_2Fe_{14}{}^{11}B$	27.6	30.5	34.7	543	545	543	135.5	3.1

hard-axis data plotted in Fig.4 are therefore taken by rotating the sample 90° away from the easy-axis direction. As our magnetometers were limited to magnetic fields of 6 T, we used linear extrapolation of the data at high fields to obtain our values of H_A. With 38% Ce doping, the saturation magnetization, M_s, decreases only 9.2% at 300 K (30.5 μ_B/f.u. for $(Nd_{0.62}Ce_{0.38})_2Fe_{14}B$ vs. 33.6 μ_B/f.u. for the undoped $Nd_2Fe_{14}B$). For comparison, the 300 K saturation magnetization of the end member $Ce_2Fe_{14}B$ compound is 23.9 μ_B/f.u. [8]. At 300 K the value of $\mu_0 H_A$ drops from an undoped value of 7.5 T to a still respectable 5.2 T for our highest achievable Ce concentration (Figure 4, inset). In (Table 5) we also list values of M_s for magnetization measurements collected at 5 K and 400 K.

4. First Principles Calculations

The $R_2Fe_{14}B$ class of materials (where R = Nd, Gd, Y etc.) has been the subject of many theoretical studies [37, 38, 39, 40, 41]. With respect to $Nd_2Fe_{14}B$, first principles studies have been used to understand the effect of partial substitution of the Nd site by various rare earth elements (e.g., Y, La, Dy, Tb etc. [42, 43]) as well as the Fe site by Si, Ge, Sn etc.[44]. In this report we calculate the effects of Ce substitution for Nd on the magnetic properties of $(Nd_{1-x}Ce_x)_2Fe_{14}B$, focusing on the parameters relevant to high performance magnetic materials: saturation magnetization, Curie temperature and magnetocrystalline anisotropy.

$Nd_2Fe_{14}B$ crystallizes in a tetragonal structure with four formula units per unit cell. In the atomic valence configuration the four electrons in the Nd-4f orbitals and the six in the Fe-3d orbitals make these ions strongly magnetic. The density of states (DOS) for $Nd_2Fe_{14}B$ in the ferromagnetic state is shown in the blue curves in Fig. 5. Comparing the total DOS with partial DOS in the lower panels, we can see that the states near the Fermi level predominantly consist of Fe-d and Nd-f states. There is an exchange splitting of ~2 eV in the Fe-d states with a nearly fully occupied spin-up channel. The spin down channel has close to two electrons, suggesting a spin magnetic moment of ~3 μ_B at the Fe sites, which is significantly above the value for bcc Fe (~2.2 μ_B/Fe).

At the Nd sites, the 4f states are empty in the spin-up channel and are partially occupied in the spin-down channel, showing that in this calculation the Nd moments point in the opposite direction compared to the Fe moments. The exchange splitting at the Nd-f DOS is similar to that of Fe-d orbitals, even though the f DOS is substantially narrower. Counting the states in the Nd-$f\downarrow$ channel up to the Fermi level gives 3.1 electrons, which suggest a spin magnetic moment of -3.1 μ_B at the Nd sites. From our calculations, we also find an orbital moment of 2.8 μ_B at the Nd-f states (opposite to the spin moment, as expected from Hund's rules), while the orbital moments at the Fe sites are ~0.06 μ_B. Spin magnetic moments calculated by integrating charge density around the atom sites agree well with the above estimates. Integrating the spin-polarized charge density around the ions, we find average spin moments of (in μ_B) -3.4, 2.5 and -0.17 for Nd, Fe and B sites respectively. The Fe moment value is larger than that for pure Fe, contributing to the excellent magnetic properties of this compound. For comparison, the experimental neutron diffraction data collected at 300 K shows Fe having net moments between 1.3 and 3.2 μ_B, bracketing the theoretical prediction; the weighted average of the experimentally-determined Fe moments is 2.39, in excellent agreement with the theoretical prediction of 2.5 μ_B. Consistent with the experimental neutron diffraction data, we find that the Fe ions bonded with B atoms were found to have a reduced moment of 1.98 μ_B. However, the net magnetic moment at the rare-earth site is -0.6 μ_B from calculation, which is quite different from the experimental value of 1.6-2.4 μ_B. This is probably a limitation of the theoretical calculation, since the 4f states are difficult to treat correctly in pseudopotential methods. The net spin+orbital (J = S+L) magnetic moment of this system is 30.3 μ_B per unit cell, in good agreement with both the neutron diffraction refinements and the magnetization data.

To understand the effect of Ce doping at the Nd sites on the properties of $Nd_2Fe_{14}B$, we replaced 10% of the Nd atoms at each crystallographic site by Ce using

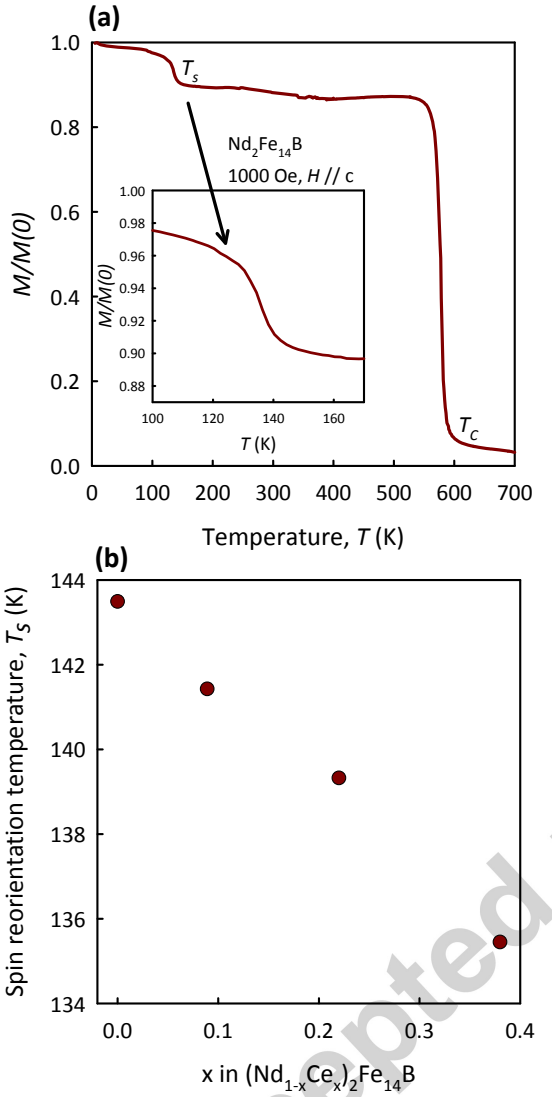

Figure 3: (a) Normalized Magnetization as a function of temperature for the undoped $Nd_2Fe_{14}B$ sample taken using 1000 Oe showing both the Curie and spin reorientation temperatures (T_C and T_s, respectively) and (b) Evolution of spin reorientation temperature as a function of Ce concentration.

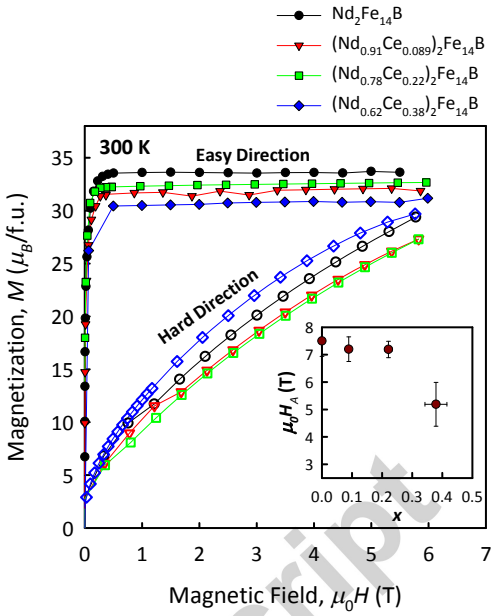

Figure 4: M(H) curves for undoped and Ce-substituted $Nd_2Fe_{14}B$ samples at 300 K. The inset displays the anisotropy field, $\mu_0 H_A$, as a function of doping. Appropriate demagnetization factors have been applied to the magnetization data based on the sample geometries.

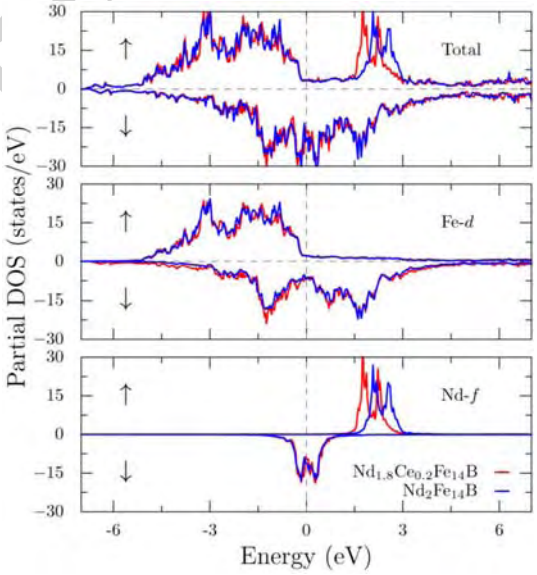

Figure 5: The total and partial density of states for undoped Nd-Fe-B (blue) and Ce doped Nd-Fe-B (red) from first-principles calculations in the ferromagnetic spin configuration. The positive and negative DOS values correspond to spin-up and spin-down channels respectively. The DOS around Fermi level is dominated by Fe-d (middle panel) and Nd/Ce-f (bottom panel) states.

the virtual crystal approximation (VCA). The total and partial DOS for the doped system are presented as red curves in Fig. 5. As we can see, the only significant change in the DOS is at the RE-f $\uparrow$ states, which are shifted to lower energies by ~0.5 eV. Thus, we see that the electronic properties of the Nd-Fe-B magnets are not significantly affected by Ce doping, except a small reduction in the magnetic moments at the Nd/Ce site since Ce has two fewer electrons in its valence shells than

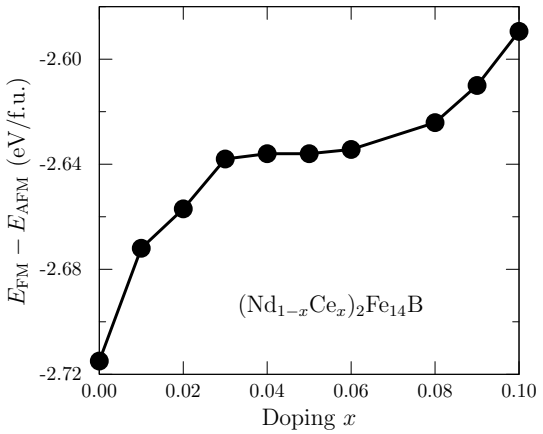

Figure 6: Variation of energy difference between ferromagnetic and hypothetical antiferromagnetic structures in $Nd_2Fe_{14}B$ as function of doping parameter *x*. The energy difference reduces upon Ce doping, suggesting that the exchange interaction *J* and consequently T_C will reduce as a function of Ce concentration.

Nd. Thus, the number of electrons in the 68 atom (8 rare earth atoms) unit cell is reduced by 1.6 electrons by 10% Ce substitution which lead to a subsequent reduction in the average 0 K magnetic moment at these sites to 3.2 μ_B from 3.4 μ_B. This reduction in RE moment is obviously responsible for the reduction in saturation magnetization seen with Ce substitution. We find from these spin-polarized calculations that the Fe moments are mostly unaffected by the substitution.

An important consequence of the reduced exchange splitting is a reduction in Curie temperature, T_C. Generally, for a ferromagnetic system characterized by large local moments such as the 2-14-1 materials, the Curie temperature is controlled by the difference in energy between the ferromagnetic ground state and an essentially antiferromagnetic structure constructed so that most of the neighbors of Fe atoms are antiparallel. This in turn is a function of the exchange parameters J_{ij} connecting nearest neighbors *i* and *j*. In the simplest mean-field approximation one may estimate the Curie temperature as a third of this energy difference, measured on a per Fe basis.

We calculated the energy difference between the above-described ferromagnetic structure and an approximate hypothetical antiferromagnetic structure obtained by flipping most of the nearest neighbor moments. The calculated energy difference is plotted in Fig. 6 as a function of the Ce concentration, *x*. The $x = 0$ value of -2.71 eV per formula unit corresponds in the mean-field approximation to a T_C of 748 K, which is to be compared to the experimental value of 584 K. The smaller experimental value suggests that effects beyond our simple mean-field approach may be relevant. A similar calculation overestimate was also presented by Alam *et al.* [10]. Upon substituting Ce atoms via VCA, the magnitude of the energy difference decreases by about 4 percent for a 10 percent Ce substitution. This suggests that the mean field *J* decreases in $Nd_2Fe_{14}B$ as *x* is increased which would in turn decrease the Curie temperature. This is consistent with our experimental results, which also find a decrease in Curie temperature with Ce alloying.

Finally, we calculated the magnetic anisotropy energy (MAE) of $(Nd_{1-x}Ce_x)_2Fe_{14}B$ for Ce concentrations $x = 0$ and $x = 0.1$ to understand the effect of doping on this important parameter. We used the experimental structure at room temperature (i.e., in the ferromagnetic state) to perform these calculations [7]. The total energy is then calculated in the presence of spin orbit coupling with the moments pointing along *a* and *c* directions. The MAE is defined as $K_1 = E_a - E_c$. We find that for $x = 0$, K_1=12.3 meV/f.u. (~8 MJ/m^3). This is somewhat larger than our experimental value of 4.9 MJ/m^3 as determined in Table 5. Overestimation of calculated MAE is expected, since it corresponds to hypothetical ferromagnetic structure at 0 K and does not account fo the canting of the moments observed below the spin reorientation temperature. We also note that temperature effects are known to be significant in this compound,[45] which would also contribute to the discrepancy between the calculated and observed MAE. We find the anisotropy energy increases slightly upon doping, leading to K_1=13.2 meV/f.u. at x = 0.1. This small increase is probably not significant considering the approximations involved in the calculations. We note that our experimental data suggest a modest decrease in $K_1$of 8% seen in the similar composition of $(Nd_{0.91}Ce_{0.089})_2Fe_{14}{}^{11}B$ (Table 5).

5. Conclusions

Large single crystals of $(Nd_{1-x}Ce_x)_2Fe_{14}B$ were grown from Ce-Nd-Fe flux. The largest of these crystals were a maximum of ~1 g in mass and displayed sharp faceting. Cerium substitution was attempted for Nd; the maximum degree of substitution we were able to achieve corresponded to the composition $(Nd_{0.62}Ce_{0.38})_2Fe_{14}B$, a value larger than Pathak *etal.* [4]. Single crystal neutron diffraction showed that the Ce has a preference for the larger RE 4*g* site, favoring this location by a factor of ~7:3 over the RE 4*f* site. The observed weak dependence of $T_s$on Ce content suggests that the RE(4*g*) site preferred by Ce does not play

a role in the spin reorientation, consistent with previous predictions[9, 22].

The presence of Ce only slightly affects magnetic properties such as T_C, M_s, and H_A. The values of these characteristics largely fall in line with empirical predictions based on the application of simple alloying rules between the two parent compounds ($Nd_2Fe_{14}B$ and $Ce_2Fe_{14}B$). The ability to synthesize large single crystals enables elucidation of important fundamental magnetic and structural properties.

We have also used X-ray photoelectron spectroscopy and synchrotron emissions to determine the oxidation states and binding energies of all species in Ce-substituted $Nd_2Fe_{14}B$; preliminary data shows that the XPS spectrum for the Ce 3*d* electrons most closely resembles that of Ce_2O_3.

With the help of first-principles calculations, we studied the electronic and magnetic properties of Ce doped Nd-Fe-B magnets. We find that for up to $x = 0.1$ doping of Ce, the electronic structure around the Fermi level is not significantly affected. The exchange splitting and the magnetic moments at the Nd sites are diminished as a consequence of Ce doping, which in turn reduces the Curie temperature. Finally, we find that the high magnetic anisotropy energy of the Nd-Fe-B system is not significantly altered by the Ce doping, confirming the experimental observations. The next step in determining the precise interactions that account for the superior properties of the compositions investigated by Pathak *et al*. [4] will involve the synthesis and characterization of Ce and Co co-doped $Nd_2Fe_{14}B$ single crystals. We have indeed synthesized these crystals and will report on them in our next publication.

Acknowledgements

The authors of this report wish to thank A.F. May for helpful discussions. In addition, the authors acknowledge the assistance of P.C. Canfield and J.A. Kolopus in the obtaining and preparation of the Ta crucibles required for single crystal growth, respectively. M.A.S., B.I.S., G.M.V., D.S.P., and B.C.S. were supported by the United States Department of Energy, Basic Energy Sciences, Materials Sciences and Engineering Division. M.A.M. acknowledges support from the United States Department of Energy, Office of Energy Efficiency and Renewable Energy, Vehicle Transportation Office, Propulsion Materials Program. The data collected at ORNLs High Flux Isotope Reactor (H.C.) and Spallation Neutron Source (B.C.C.) were sponsored by the Scientific User Facilities Division, Office of Basic Energy Sciences, United States Department of Energy. B.S.C., K.V.S., and D.S.P. acknowledge support from the Critical Materials Institute, an Energy Innovation Hub, funded by the U.S. Department of Energy, Office of Energy Efficiency and Renewable Energy, Advanced Manufacturing Office. The Advanced Light Source is supported by the Director, Office of Science, Office of Basic Energy Sciences, of the U.S. Department of Energy under Contract No. DE-AC02-05CH11231.

References

[1] United States Department of Energy , Office of Public Policy and International Affairs. Critical materials strategy. *Technical Report*, 2011.

[2] M. Sagawa, S. Fujimura, H. Yamamoto, Y. Matsuura, and K. Hiraga. Permanent magnet materials based on the rare earth-iron-boron tetragonal compounds. *IEEE Transactions on Magnetics*, MAG-20:1584–9, 1984.

[3] J. J. Croat, J. F. Herbst, R. W. Lee, and F. E. Pinkerton. Praseodymium-iron- and neodymium-iron-based materials: A new class of high-performance permanent magnets. *Journal of Applied Physics*, 55:2078–82, 1984.

[4] A. K. Pathak, M. Khan, K. A. Gschneidner, Jr., R. W. McCallum, L. Zhou, K. Sun, K. W. Dennis, C. Zhou, F. E. Pinkerton, M. J. Kramer, and V. K. Pecharsky. Cerium: An unlikely replacement of dysprosium in high performance Nd–Fe–B permanent magnets. *Advanced Materials*, 27:2663–2667, 2015.

[5] D. Givord, H. S. Li, and J. M. Moreau. Magnetic properties and crystal structure of neodymium-iron-boron ($Nd_2Fe_{14}B$). 50:497–9, 1984.

[6] J. F. Herbst, J. J. Croat, F. E. Pinkerton, and W. B. Yelon. Relationships between crystal structure and magnetic properties in neodymium-iron-boron ($Nd_2Fe_{14}B$). *Physical Review B*, 29:4176–8, 1984.

[7] C. B. Shoemaker, D. P. Shoemaker, and R. Fruchart. The structure of a new magnetic phase related to the sigma phase: Iron neodymium boride $Nd_2Fe_{14}B$. *Acta Crystallographica, Section C*, C40:1665–8, 1984.

[8] J. F. Herbst. Rare earth(R) iron boron ($R_2Fe_{14}B$) materials: Intrinsic properties and technological aspects. *Reviews of Modern Physics*, 63:819–98, 1991.

[9] C. Abache and J. Oesterreicher. Magnetic anisotropies and spin reorientations of $R_2Fe_{14}B$-type compounds. *Journal of Applied Physics*, 60:3671–9, 1986.

[10] A. Alam, M. Khan, R. W. McCallum, and D. D. Johnson. Site-preference and valency for rare-earth sites in $(R\text{-}Ce)_2Fe_{14}B$ magnets. *Applied Physics Letters*, 102:042402/1–042402/4, 2013.

[11] K. A. Gschneidner, M. Khan, R. W. McCallum, V. K. Pecharsky, A. K. Pathak, L. Zhou, D. Brown, F. E. Pinkerton, and C. Zhou. Dy-free, reduced Nd, high performance $Nd_2Fe_{14}B$-based permanent magnets. *Proceedings of the 23rd International Workshop on Rare-Earth and Future Permanent Magnets and Their Applications (REPM 2014), Annapolis, Maryland, USA*, pages 403–406, 2014.

[12] P. C. Canfield and I. R. Fisher. High-temperature solution growth of intermetallic single crystals and quasicrystals. *Journal of Crystal Growth*, 225:155–161, 2001.

[13] L. H. Lewis, J.-Y. Wang, and P. Canfield. Magnetic domains of single-crystal $Nd_2Fe_{14}B$ imaged by unmodified scanning electron microscopy. *Journal of Applied Physics*, 83:6843–6845, 1998.

[14] G. M. Sheldrick. A Short History of *SHELX*. *Acta Crystallographica Section A*, 64(1):112–122, 2008.

[15] B. C. Chakoumakos, H. Cao, F. Ye, A. D. Stoica, M. Popovici, M. Sundaram, W. Zhou, J. S. Hicks, G. W. Lynn, and R. A. Riedel. Four-Circle Single-Crystal Neutron Diffractometer at the High Flux Isotope Reactor. *Journal of Applied Crystallography*, 44(3):655–658, 2011.

[16] J. Rodriguez-Carvajal. Recent advances in magnetic structure determination by neutron powder diffraction. *Physica B*, 192(12):55 – 69, 1993.

[17] S. Axnanda, E. J. Crumlin, S. Rani, Z. Hussain, B. Mao, R. Chang, P. G. Karlsson, Marten O. M. E., M. Lundqvist, R. Moberg, P. Ross, and Z. Liu. Using "tender" x-ray ambient pressure x-ray photoelectron spectroscopy as a direct probe of solid-liquid interface. *Scientific Reports*, 5:9788, 2015.

[18] J. P. Perdew, K. Burke, and M. Ernzerhof. Generalized gradient approximation made simple. *Phys. Rev. Lett.*, 77:3865–3868, 1996.

[19] P. E. Bloechl. Projector augmented-wave method. *Physical Review B*, 50:17953–79, 1994.

[20] G. Kresse and J. Hafner. *Ab Initio* molecular dynamics of liquid metals. *Physical Review B*, 47:558–61, 1993.

[21] G. Kresse and J. Furthmueller. Efficient iterative schemes for *Ab Initio* total-energy calculations using a plane-wave basis set. *Physical Review B*, 54, 1996.

[22] C. Abache and H. Oesterreicher. Magnetic properties of compounds rare earth-iron-boron ($R_2Fe_{14}B$). *Journal of Applied Physics*, 57:4112–14, 1985.

[23] J. F. Herbst and W. B. Yelon. Preferential site occupation and magnetic structure of $Nd_2(Co_xFe_{(1-x)})_{14}B$ systems. *Journal of Applied Physics*, 60(12):4224–4229, 1986.

[24] G. Dong, Y. Sui, P. Qian, Y. Wu, and L. Guo. Experimental and theoretical studies on site preference of Ti in $Nd_2(Fe, Ti)_{14}B$. *Journal of Magnetism and Magnetic Materials*, 379:108 – 111, 2015.

[25] A.E. Teplykh, Yu.G. Chukalkin, S. Lee, S.G. Bogdanov, N.V. Kudrevatykh, E.V. Rosenfeld, Y.N. Skryabin, Y. Choi, A.V. Andreev, and A.N. Pirogov. Magnetism of ordered and disordered alloys of $R_2Fe_{14}B$ (R = Nd, Er) type. *Journal of Alloys and Compounds*, 581:423 – 430, 2013.

[26] A. Gagin and I. Levin. Accounting for unknown systematic errors in rietveld refinements: a bayesian statistics approach. *J. Appl. Cryst.*, 48:1201–1211, 2015.

[27] J. F. Herbst and W. B. Yelon. Crystal and magnetic structure of praseodymium iron boride ($Pr_2Fe_{14}B$) and dysprosium iron boride ($Dy_2Fe_{14}B$). *J. Appl. Phys.*, 57:2343–5, 1985.

[28] O. Isnard and D. Fruchart. Magnetism in Fe-based intermetallics: relationships between local environments and local magnetic moments. *J. Alloys Compd.*, 205:1–15, 1994.

[29] F.C. Frank and J.S. Kasper. Complex alloy structures regarded as sphere packings. II. Analysis and classification of representative structures. *Acta Cryst.*, 12:483–499, 1959.

[30] F.C. Frank and J.S. Kasper. Complex alloy structures regarded as sphere packings. I. Definitions and basic principles. *Acta Cryst.*, 11:184–190, 1958.

[31] O. Isnard, W. B. Yelon, S. Miraglia, and D. Fruchart. Neutron-diffraction study of the insertion scheme of hydrogen in $Nd_2Fe_{14}B$. *J. Appl. Phys.*, 78:1892–8, 1995.

[32] E. T. Teatum, K. A. Gschneidner, Jr., and J. T. Waber. Compilation of calculated data useful in predicting metallurgical behavior of the elements in binary alloy systems. Technical report, Los Alamos Sci. Lab., 1968.

[33] P. Wolfers, M. Bacmann, and D. Fruchart. Single crystal neutron diffraction investigations of the crystal and magnetic structures of R_2Fe_14B (R = Y, Nd, Ho, Er. *J. Alloys Compd.*, 39:483–499, 1959.

[34] A. K. Pathak, M. Khan, K. A. Gschneidner, Jr., R. W. McCallum, L. Zhou, K. Sun, M. J. Kramer, and V. K. Pecharsky. Magnetic properties of bulk, and rapidly solidified nanostructured $(Nd_{1-x}Ce_x)_2Fe_{14-y}Co_yB$ ribbons. *Acta Mater.*, 103:211–216, 2016.

[35] M. Sagawa, S. Fujimura, H. Yamamoto, Y. Matsuura, and S. Hirosawa. Magnetic properties of rare earth-iron-boron permanent magnet materials. *J. Appl. Phys.*, 57:4094–6, 1985.

[36] M. Yamada, H. Kato, H .and Yamamoto, and Y. Nakagawa. Crystal-field analysis of the magnetization process in a series of neodymium iron boride ($Nd_2Fe_{14}B$)-type compounds. *Phys. Rev. B*, 38:620–33, 1988.

[37] Z. Gu and W. Y. Ching. Comparative studies of electronic and magnetic structures in yttrium iron boride ($Y_2Fe_{14}B$), neodymium iron boride ($Nd_2Fe_{14}B$), yttrium cobalt boride ($Y_2Co_{14}B$), and neodymium cobalt boride ($Nd_2Co_{14}B$). *Physical Review B*, 36:8530–46, 1987.

[38] S. S. Jaswal. Electronic structure and magnetism of $R_2Fe_{14}B$ (R = yttrium, neodymium) compounds. *Physical Review B*, 41:9697–700, 1990.

[39] B. I. Min, J. S. Kang, J. H. Hong, J. I. Jeong, Y. P. Lee, S. D. Choi, W. Y. Lee, C. J. Yang, and C. G. Olson. Electronic and magnetic structures of the rare-earth permanent magnet neodymium iron boride ($Nd_2Fe_{14}B$). *Physical Review B*, 48:6217–24, 1993.

[40] L. Nordstroem, B. Johansson, and M. S. S. Brooks. Calculation of the electronic structure and the magnetic moments of neodymium iron boride ($Nd_2Fe_{14}B$). *Journal of Physics: Condensed Matter*, 5:7859–70, 1993.

[41] I. Kitagawa and Y. Asari. Magnetic anisotropy of $R_2Fe_{14}B$ (R=Nd, Gd, Y): Density functional calculation by using the linear combination of pseudo-atomic-orbital method. *Physical Review B*, 81:214408/1–214408/7, 2010.

[42] X. B. Liu and Z. Altounian. The partitioning of Dy and Tb in NdFeB magnets: A first-principles study. *Journal of Applied Physics*, 111, 2012.

[43] X. B. Liu, Z. Altounian, M. Huang, Q. Zhang, and J. P. Liu. The partitioning of La and Y in Nd-Fe-B magnets: A first-principles study. *Journal of Alloys and Compounds*, 549:366–369, 2013.

[44] X. B. Liu, J. P. Liu, Q. Zhang, and Z. Altounian. The Fe substitution in $Nd_2(Fe,M)_{14}B$ (M = Si, Ge and Sn): A first-principles study. *Computational Materials Science*, 85:186–192, 2014.

[45] D. Goll and H. Kronmuller. High-performance permanent magnets. *Naturwissenschaften*, 87:423–438, 2000.